Turkish Journal of Earth Sciences
http://journals.tubitak.gov.tr/earth/
Research Article

Turkish J Earth Sci
(2013) 22: 398-413

doi:10.3906/yer-1112-12

Late Holocene climatic oscillations traced by clay mineral assemblages and other palaeoceanographic proxies in Ria de Vigo (NW Spain)

Virgínia MARTINS[1,2,*], Fernando ROCHA[1], Cristina SEQUEIRA[1], Paula MARTINS[1], José SANTOS[1], João A. DIAS[3], Olivier WEBER[4], Jean-Marie JOUANNEAU[4], Belén RUBIO[5], Daniel REY[5], Ana BERNABEU[5], Eduardo SILVA[1], Lazaro LAUT[6], Rubens FIGUEIRA[7]

[1]GeoBioTec Research Centre, Department of Geosciences, University of Aveiro, Campus de Santiago, 3810-193 Aveiro, Portugal (E-mail: virginia.martins@ua.pt)

[2]CESAM, Department of Geosciences, University of Aveiro, Campus de Santiago, 3810-193 Aveiro, Portugal

[3]CIMA, Algarve University, Campus de Gambelas, Faro, Portugal

[4]Department of Geology and Oceanography, University of Bordeaux I/CNRS, France

[5]Department of Marine Geosciences, University of Vigo, 36310 Vigo, Spain

[6]Natural Science Department, Federal University of the State of Rio de Janeiro – UNIRIO, Brazil

[7]Oceanographic Institute, São Paulo University, Brazil

Received: 29.12.2011 • **Accepted:** 19.09.2012 • **Published Online:** 06.05.2013 • **Printed:** 06.06.2013

Abstract: This work aims to study recent climatic oscillations and their influence on sedimentation in the Ria de Vigo, a coastal embayment in Galicia, NW Spain. It is based on the study of clay mineral assemblages, in conjunction with other proxies (granulometric, geochemical, geochronological and microfaunal), in the core KSGX 24. A Benthic Foraminifera High Productivity (BFHP) proxy was used to determine changes in the flux of organic matter (OM) at the bottom of the study area. Total organic carbon (TOC) content is not a suitable proxy to estimate changes in the past supply of OM due to diagenetic processes. The sedimentation was finest in 3 sections: ~ 230–214 cm, ~ 185–73 cm and ~ 20–0 cm. These muddy sections are characterised, in general, by higher proportions of detrital minerals, concentrations of several chemical elements related to lithogenic sources and BFHP values. In addition, these sections are impoverished in carbonates, Ca, Sr and La when compared with the layers with the highest sand content. The clay mineral assemblage of the studied site, characterised by the dominance of illite, intermediate concentrations of kaolinite and minor amounts of smectite and chlorite, reveals the prevalence of a typical temperate humid climate in the last 3 ka BP, the estimated age for the core base. However, the quantities of illite and chlorite increase in the muddy layers. The characteristics of these muddy layers were interpreted as representing relatively cold climatic oscillations associated with the strengthening of northerly winds and the prevalence of an upwelling regime corresponding to well-known periods, such as the first cold period of the Upper Holocene (~ 2.9 ka cal BP), the Dark Ages (between ~ 2.2 - 1.2 ka cal BP) and the Little Ice Age (~ 0.6 ka cal BP).

Key Words: Paleoclimatology, historical climatic oscillations, benthic foraminifera, multiproxy approach, upwelling

1. Introduction

The composition and proportions of individual clay minerals in mid-latitude marine sediments depend on climatic conditions on land, the nature of the source rocks, the transport agents and the depositional setting (Chamley 1989 and references therein). The clay mineralogy of sediments can provide important information that helps in the reconstruction of climatic signals (Bischoff *et al.* 1997; Menking 1997; Yuretich *et al.* 1999; Bischoff & Cummins 2001; Thamban *et al.* 2002; Yuretich & Ervin 2002; Jason *et al.* 2005; Diekmann *et al.* 2008), especially in combination with other proxies.

In this study clay mineral assemblages, combined with other palaeoenvironmental data, were studied in a core recovered from the outer sector of the Ria de Vigo, a temperate coastal embayment located in the north-west of the Iberian Peninsula, Galicia, Spain, and used to improve our knowledge of recent climatic oscillations and their influence on the oceanographic processes and coastal systems of this region.

This is an important topic because the Galician continental margin is a sensitive climatic area located in the north-eastern Atlantic Ocean, at the boundary of where the sedimentary sequences record oceanographic

* Correspondence: virginia.martins@ua.pt

changes in response to rapid climatic oscillations (Diz *et al.* 2002; Desprat *et al.* 2003; González-Álvarez *et al.* 2005; Martins *et al.* 2006a, 2006b, 2007; Bernárdez *et al.* 2008; Andrade *et al.* 2011). These studies can be useful for predicting future climatic changes.

There are very few studies covering detrital clay assemblages on the Galician coast (Belzunce-Segarra *et al.* 2002). These studies have shown that clay minerals are delivered from the surrounding land masses and supplied by the major river systems and coastal erosion.

2. Study area

Galicia, in NW Spain, has one of the most complex littoral environments of the NW Iberian Peninsula, with 4 coastal incised valleys invaded by the sea. The Galician Rias Baixas, located between 42°N and 43°N, were formed in the Tertiary era as a consequence of the reactivation of ancient Variscan faults, giving rise to tectonic sunken valleys that were later invaded by the sea (Torre 1958; Vidal Romani 1984).

The Rias Baixas are highly productive ecosystems due to coastal upwelling (Wooster *et al.* 1976). Recurrent upwelling on the NW Iberian shelf occurs, on average, from March to September when northerly winds are dominant, whereas downwelling prevails during the rest of the year (Fiúza *et al.* 1982; Blanton *et al.* 1987; Tenore *et al.* 1995; Figueiras *et al.* 2002). During the upwelling season, recurrent upwelling pulses force nutrient-rich Eastern North Atlantic Central Water (ENACW) to enter the rias. In extreme cases ENACW reaches the photic layer, causing an enhancement of primary productivity (Prego 1993; Álvarez-Salgado *et al.* 1996; Figueiras *et al.* 2002). Under the prevalence of northerly winds, the direction of currents on the shelf is southward (Peliz *et al.* 2002). In winter, storm winds, which blow predominantly from the SW, induce an Ekman transport towards the coast and the development of downwelling events (Vitorino *et al.* 2002). In winter, the oceanic currents along the slope and on the shelf flow northwards (Haynes & Barton 1990).

The Ria de Vigo, the southernmost of the Rias Baixas, has a distinctive funnel shape with a NNE–SSW orientation and occupies an area of about 176.4 km^2 (Vilas et *al.* 2005). The Ria de Vigo is separated from the Atlantic by two large islands (Isles Cíes) located at its mouth. The Isles Cíes leave two relatively narrow corridors at the northern and southern entrances, which allow its intercommunication with the ocean (Figure 1).

The water depths within the Ria de Vigo range from 7 m, at its inner shallows, to 55 m, at the outer (south-west) entrance to the sea. Its northern entrance is somewhat shallower compared to the 55 m depth of the southern entrance, with a maximum depth of 30 m (García-García *et al.* 2005).

The topography of Galicia determines the existence of an extensive hydrographical network. The Ria de Vigo receives fresh water from several rivers, but mostly from

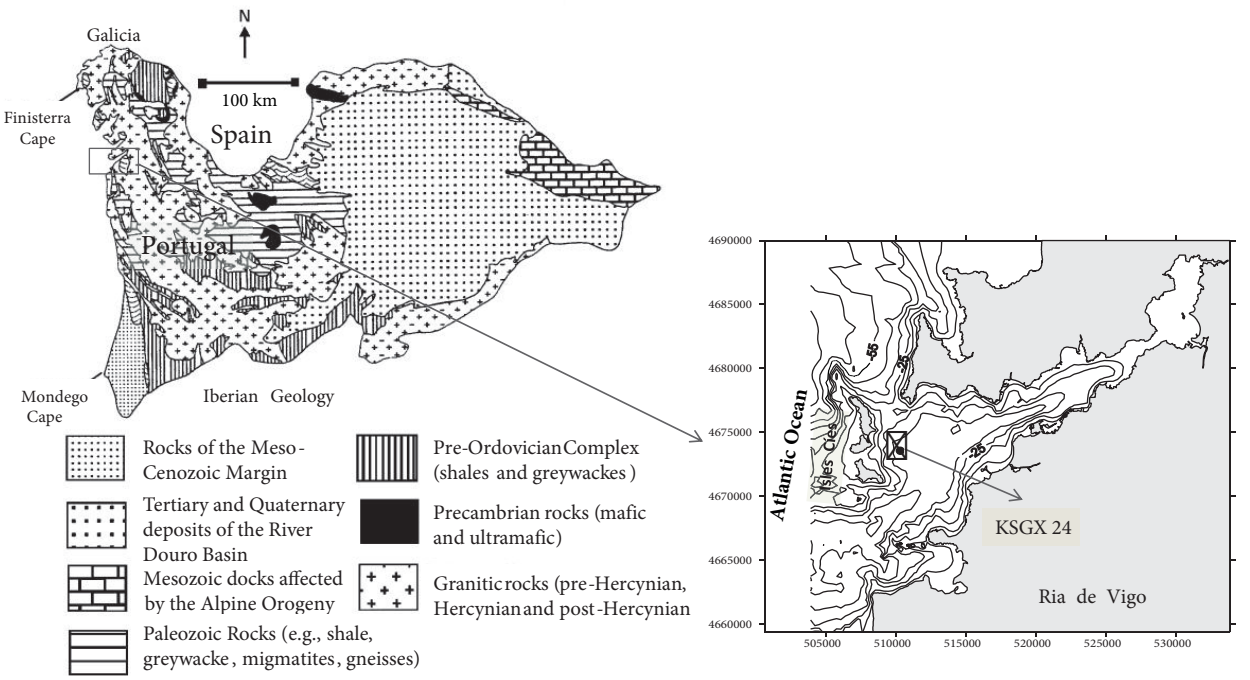

Figure 1. The geology of the northern region of the Iberian Peninsula (adapted from Julivert *et al.* 1980) and the site (42°12′48″N, 8°51′90″W, 39 m depth) where the core KSGX 24 was recovered in Ria de Vigo (Galicia, NW Spain). The bathymetry and the metric coordinates (according to the datum WGS84) of this ria are presented in this map.

the Verdugo and Oitaven that flow into San Simón Bay (Pérez-Arlucea *et al*. 2005).

The Ria de Vigo behaves as a partially mixed estuary with a 2-layered positive residual circulation pattern, maintained in winter by freshwater flow and in summer by the upwelling oceanographic regime (Prego & Fraga 1992). The mountainous strip that runs parallel to the coast has high annual precipitation. In general, maximum rainfall occurs in December–January, with a secondary peak sometime around April, while minimum rainfall is found in July. On the whole, the period of low water flow extends from July to October, while high water flow occurs between January and March and, exceptionally, extends into May (Martínez-Ansemil & Membiela 1992). The high fluvial fresh water inflow can produce stratification in the water column of the ria (Diz *et al*. 2002).

3. Methods and materials

The OMEX (Ocean Margin Exchange Project) gravity core KSGX 24 (236 cm long), taken in the outer sector of the Ria de Vigo near the Isles Cíes (42°12′48″N, 8°51′90″W, 39 m depth; Figure 1), was studied in this work. This core was sampled at each centimetre along its length. Mineralogical and textural studies were performed at each centimetre. Geochemical and microfaunal (benthic foraminifera) studies were analysed in samples spaced 2 cm apart.

Mineralogical studies were carried out on the <63 μm (silt) and <2 μm (clay) fractions of the sediments through X-ray diffraction (XRD) using Philips PW1130/90 and X'Pert PW3040/60 equipment and Cu Kα radiation. Scans were run between 2° and 40° 2θ. Qualitative and semiquantitative mineralogical analyses followed the method described by Martins *et al*. (2007). For the purposes of XRD, performed on oriented clay samples, about 3 g of fine sediment fraction of each sample were first decomposed (disaggregated by ultrasonic vibration for 1 min) and then left to stand for 20 min so that all particle sizes greater than clay-sized (<2 μm) would settle to the bottom of the tube and leave the clay particles in suspension (according to Stoke's law). The suspension was removed and oriented, and dried clay preparations were made. The first slide was air-dried while the second was saturated with ethylene glycol. The third slide was analysed after heating to 550 °C for 2 h, at which temperature kaolinite and certain chlorites are destroyed. The 4 principal clay mineral groups were identified by their basal spacing at 0.7 nm (kaolinite, chlorite), 1.0 nm (illite), 1.5–1.7 nm (smectite) and 1.4 nm (chlorite). Chlorite (004) was identified at 0.354 nm and kaolinite (002) at 0.358 nm (Biscaye 1964); for semiquantification, peak areas of their specific reflections were calculated and weighted by empirically estimated factors (Galhano *et al*. 1999; Oliveira *et al*. 2002).

The sum of the percentage of all minerals determined in each diffractogram is 100%. However, fine or clay fractions correspond to a proportion of the total sediment of each sample. Thus, in this work, the percentage of each mineral, evaluated from the diffractograms analysis, was recalculated according to the percentage of fine and clay fractions along the core, respectively.

A laser microgranulometer (Mastersizer S instrument, Malvern Instruments) was used for determining grain-size distribution of the sediments in each sample.

Concentrations of Al, As, Ca, Co, Cr, Fe, Ga, K, La, Li, Ni, S, Sc, Sr, V and Zn were determined at ACME Analytical Laboratories, Canada. The analysis was done after the total digestion of sediment with 4 acids ($HClO_4$ – HNO_3 – HCl – HF) followed by inductively coupled plasma–mass spectrometry (ICP–MS) analysis. The accuracy of the analysis is generally greater than 95%.

TOC was analysed by combustion in an LECO CS 125 analyser, using the method of Jouanneau *et al*. (2002).

Benthic foraminifera assemblages were determined in the >63 μm sediment fraction, considering the proportion of each species, using at least 300 specimens per sample. The Benthic Foraminifera High Productivity (BFHP) index was used in this core to discriminate periods of high supply of organic matter (OM) to the sea floor. This microfaunal proxy includes the total percentage of species related to a high and sustainable flux of metabolisable OM and was determined following the procedure of Martins *et al*. (2006a, 2006b, 2007). This proxy was used because the sedimentary content in total organic carbon (TOC) is not a good method to evaluate past changes in the supply of organic material to the sediment. OM suffers rapid mineralisation caused by aerobic activity of benthic organisms in the oxic layers near the water–sediment interface, being buried a relatively refractory fraction (Jouanneau *et al*. 2002). Thus, BFHP can be a useful proxy to identify changes in the flux of OM to the bottom when dead benthic foraminiferal assemblages are well preserved.

Four radiocarbon ages of mixed foraminifera tests (10 mg to 20 mg) were determined from the >125 μm size fraction of selected layers (33–34 cm, 71–72 cm, 143–144 cm and 193–194 cm) and were carried out by Beta Analytic Inc., Miami, Florida, USA, using the AMS method. Radiocarbon ages were calibrated to calendar years before present (cal ka BP) using the calibration program Calib 6.0 (by M. Stuiver, P.J. Reimer and R.W. Reimer) in conjunction with the method of Stuiver and Reimer (1993). Radiocarbon ages were not corrected for the reservoir effect, since the ΔR evaluated for this region for the late Holocene is quite variable (Soares & Dias 2007).

Correlations between variables and principal component analysis were performed using STATISTICA 7.0 software.

4. Results

4.1. Ages and composition of sediments

Results for radiocarbon ages are presented in Table 1. The dating model of this core was based on 2 sigma calibrated (cal) before present (BP). Based on these results, an age of about ~ 3 ka cal BP is estimated for the core base (Figure 2). The average sedimentation rates (Table 2), based on the measured radiocarbon age, were obtained by linear interpolation. These data are comparable with other cores studied in the Ria de Vigo (Mohamed *et al*. 2011), where sedimentation rates in the outer sector decreased from 100 cm kyr^{-1} at the base to about 50 cm kyr^{-1} at the core top.

This core is composed of muddy sediments with mean grain size varying between 13 and 26 μm. Fine fraction (<63 μm) represents 76%–93% of the bulk sediment. Fine silt and clay fractions (<15 μm) varied between 25% and 52% in the core.

The results of XRD semiquantification of the mineralogical composition of the fine and clay fractions revealed that the sediments are composed mainly of quartz (17%–42%), phyllosilicates (11%–49%, mainly muscovite, biotite and illite), feldspars (10%–27%) and calcite (<22%). Minor components (<11%) include opal C/T, anatase, siderite, dolomite and pyrite, which is present throughout the core. The mineralogy of the clay fractions shows a predominance of illite (6%–30%) and kaolinite (3%–15%) assemblages throughout the core. Minor chlorite (1%–16%) and layers composed of a mix of smectite + illite–smectite, randomly distributed, were also identified (<6%).

TOC values in the first 40 cm of the core vary (according to Jouanneau *et al*. 2002) between 1.95% and 1.50% (Table 3). The median and range of element concentrations are shown in Table 4. Values of the main variables analysed in this study, including granulometric, mineralogical and geochemical data as well as the BFHP index, taken at each 2 cm along the core, are shown in Table 5.

A total of about 200 benthic foraminiferal taxa were identified in this core. The most frequent species are *Nonion fabum* (<38%), *Cibicides ungerianus* (<31%), *Bolivina pseudoplicata* (<22%), *Brizalina spathulata* (<22%), *Bolivina ordinaria* (<15%), *Bulimina elongata* (<14%), *Ammonia beccarii* (<14%), *Bolivina variabilis* (<12%), *Bolivina compacta* (<9%), *Elphidium gerthi* (<8%), *Asterigerinata mamilla* (>8%), *Gavelinopsis praegeri* (<8%) and *Lobatula lobatula* (<5%). Some species of benthic foraminifera found in this core display opportunistic behaviour and reflect a high and sustainable flux of OM, such as bolivinids and buliminids, as well *Nonion fabum, Ammonia beccarii*, *Rectuvigerina phlegeri*, *Elphidium gerthi*, *Hyalinea balthica*, *Nonionella stella* and *Valvulineria bradyana* (Diz *et al*. 2004, 2006; Martins *et al*. 2005 and references therein). The total relative abundance of these species was used as a BFHP proxy, aiming to identify changes in the flux of OM to the bottom of the study area. BFHP values vary between 39% and 76% within the core. The highest values occur, in general, in finer sediments.

4.2. Statistical data analysis

Principal component analysis (PCA) was used to study the covariance between the variables studied in this work. The evolution of the main factor scores, which explains 65% of data variability, is presented in Figure 3a. Results of the first 2 factors of the PCA, which explain most of data variability (70%), are plotted in Figure 3b. The first factor is related to the hydrodynamic conditions and separates 2 groups of variables: Group I, the percentage of fine fraction, illite plus chlorite, detrital minerals and BFHP, and concentrations of Al, As, Co, Cr, Fe, Ga, K, Li, Ni, S, Sc, V, and Zn; and Group II, sand fraction, carbonate minerals and concentrations of Ca, Sr, and La.

Depth plots for some of those variables are included in Figures 4–6. Three muddy sections (richer in fine fraction) are identified along this core: ~ 230–214 cm, ~ 185–73 cm and the upper ~ 20 cm. In these layers, concentrations of Al, As, Co, Cr, Fe, Ga, K, Li, Ni, S, Sc, V and Zn tend to be higher. Depth plots for Al, S, Fe, Sc and Ga are presented in Figure 5. The other chemical elements have a similar behaviour, as revealed by the positive and significant Pearson correlations between them, with Al, S, Fe, Sc and Ga and with the fine fraction (52–83, $P < 0.05$). The proportion of detrital minerals, as well as the fine-to-coarse detrital minerals ratio (Vidinha *et al.* 2007) and the BFHP values, also tend to increase at ~ 230–214 cm

Table 1. Radiocarbon dates.

Samples (cm)	Conventional radiocarbon age	Radiocarbon age (2σ calibration)	Beta analytic no.
33–34 cm	1520 ± 40 BP	1160 to 970 cal BP	20.9729
71–72 cm	1970 ± 40 BP	1610 to 1420 cal BP	164.243
143–145 cm	2440 ± 40 BP	2160 to 1980 cal BP	164.244
193–194 cm	2850 ± 40 BP	2720 to 2470 cal BP	164.245

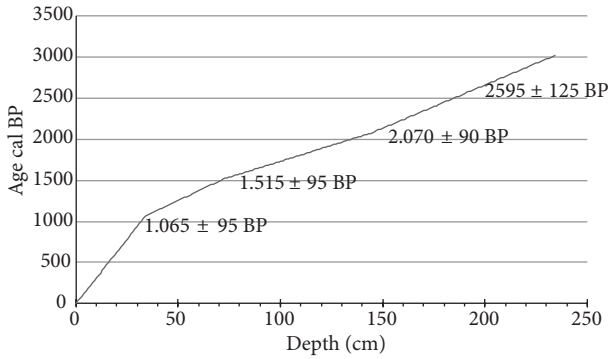

Figure 2. Age versus depth plot for the core KSGX 24. The values of four 2σ calibrated radiocarbon ages are shown.

(~ 2.9 ka cal BP), ~ 185–73 cm (~ 2.2–1.2 ka cal BP) and in the upper ~ 20 cm (from ~ 0.6 ka cal BP). Contents of carbonate minerals and concentrations of Ca, Sr and La are lowest in those sections (Figure 6).

5. Discussion

5.1. Characteristics of sedimentation in the outer sector of the Ria de Vigo during the late Holocene

The mineralogical composition of this core reveals that the sediments deposited in the outer sector of the Ria de Vigo during the late Holocene were mostly siliciclastic and related to the weathering of adjacent continental rocks. The geology of the nearby source area of the sediments is basically dominated by granite and schist (Castañón *et al.* 1981; Hurtado *et al.* 1981; Pondal *et al.* 1982). Recent sediments of the Ria de Vigo consist of terrigenous and biogenic deposits and incorporate not only material transported by the rivers from the adjacent land areas, but also products of shoreline erosion (which may be carried by marine currents from external sources), of in situ biological activity and of human activities (Rubio *et al.* 2000).

The terrigenous component of this core contains mostly detrital minerals (quartz, phyllosilicates and feldspars). The biogenic component consists of a significant amount of carbonates (mostly calcite; <22%), mainly comprising foraminifera tests and mollusc shells. Significant proportions of opal identified by XRD also provide a record of diatom frustules at the bottom of the study area. Jouanneau *et al.* (2002) determined that the amount of OM in the upper 40 cm of this core is ~ 1.5%–1.95% (Table 4). Processes involved in OM degradation by aerobic organisms led to depressed levels of oxygen in the sediments and gave way to the precipitation of diagenetic minerals such as pyrite. Pyrite is a diagenetic mineral common in anoxic environments, formed by the reaction of sulphate with the reduced form of iron (Fe^{2+}); this process is mediated by OM reaching the ria bottom, with its oxidation then following a characteristic sequence of reactions (Bender & Heggie 1984). Pyrite is present throughout the core length (Figure 4).

Both Al and Li largely occur in aluminosilicates from the continental weathering products, which are mainly introduced into the oceanic system by the rivers (Loring 1990, 1991; Araújo *et al.* 2002). Most of the other elements may also be included in or adsorbed onto mica particles or clay minerals, since all these elements have positive and significant correlations with the fine fraction and phyllosilicates, but most significantly with the sedimentary content in illite plus chlorite. For instance, higher concentrations of K may be related to the large amount of illite in these layers. Feldspars and mica are the dominant host minerals for Ga in igneous and metamorphic rocks, as they are for Al. In this core, however, the correlation between Ga and feldspars is not significantly positive, and indeed sometimes negative. Thus, Ga was probably mostly concentrated, together with Al, in mica.

The coarser layers are characterised by a more abundant sand fraction, which includes significant amounts of bioclasts composed of carbonate minerals. In the terrigenous component, there is an increase of quartz and feldspars, and a decrease of phyllosilicates, namely clay minerals. Geochemically, these layers display the highest concentrations of Ca and Sr, as expected from the abundance of carbonates, but also of La. The relatively high La concentrations may be related to the supply of minerals such as monazite [(Ce, La, Pr, Nd, Th, Y)PO_4], allanite [(Ce, Ca, Y, La)$_2$(Al, Fe^{+3})$_3$(SiO_4)$_3$(OH)] and bastnasite

Table 2. Estimation of the mean sedimentation rate.

Core sections	Mean sedimentation rate (cm kyr^{-1})
0–34 cm	30
35–72 cm	90
73–144 cm	82
144–235 cm	122

Table 3. Total organic carbon content determined for the dry sediment.

Sample	TOC (%)	Sample	TOC (%)	Sample	TOC (%)	Sample	TOC (%)
Niv:00-01	1.60	Niv:10-11	1.65	Niv:20-21	1.65	Niv:30-31	1.85
Niv:01-02	1.65	Niv:11-12	1.80	Niv:21-22	1.75	Niv:31-32	1.80
Niv:02-03	1.55	Niv:12-13	1.65	Niv:22-23	1.95	Niv:32-33	1.65
Niv:03-04	1.60	Niv:13-14	1.65	Niv:23-24	1.70	Niv:33-34	1.70
Niv:04-05	1.55	Niv:14-15	1.80	Niv:24-25	1.90	Niv:34-35	1.55
Niv:05-06	1.80	Niv:15-16	1.65	Niv:25-26	1.70	Niv:35-36	1.75
Niv:06-07	1.80	Niv:16-17	1.65	Niv:26-27	1.75	Niv:36-37	1.60
Niv:07-08	1.80	Niv:17-18	1.75	Niv:27-28	1.80	Niv:37-38	1.75
Niv:08-09	1.65	Niv:18-19	1.75	Niv:28-29	1.50	Niv:38-39	1.60
Niv:09-10	1.60	Niv:19-20	1.85	Niv:29-30	1.85	Niv:39-40	1.95

[(La, Ce, Y)CO_3F], which contain important amounts of La and other rare earth elements (REEs) and are frequently enclosed in biotite (Saleh 2007), a heavy mineral that is habitually deposited with coarse terrigenous particles.

Lanthanum and Sc have significant negative Pearson correlations in this core. Despite Sc having some affinities with REEs, its geochemical behaviour does not follow that of La since their ionic radii are quite different (Frondel 1970; Eby 1973). In igneous rocks, the REEs are concentrated in intermediate and felsic varieties, whereas Sc is more important in mafic and ultramafic lithologies (Norman & Haskin 1968). The minerals that incorporate the most significant amounts of Sc are ferromagnesian silicates, namely pyroxene [$XY(Si,Al)_2O_6$], where X represents Ca, Na, Fe^{+2} and magnesium and more rarely Zn, Mn, and Li. Y represents ions of smaller size, such as Cr, Al, Fe^{+3}, Mg, Mn, Sc, Ti, V and even Fe^{+2}, hornblende [$(Ca, Na)_{2-3}(Mg, Fe, Al)_5(Al, Si)_8O_{22}(OH,F)_2$] and biotite [$(K(Mg, Fe)_3(OH, F)_2(Al, Fe)Si_3O_{10}$], and certain accessory minerals, such as apatite, $Ca_5(PO4)_3(F, Cl, OH)$ (Tilling *et al*. 1969). In this core, Sc has a high significant positive Pearson correlation with Fe (0.93, $P < 0.05$). In several areas of Galicia and Trás-os-Montes (N Portugal), in the complexes of Cape Ortegal, Ordenes, Lalin, Bragança and Morais, basic and ultrabasic rocks are prevalent (Pondal *et al*. 1982). Ultrabasic rocks outcrop on the northern coast of Galicia (Julivert *et al*. 1980). Thus, the elevated levels of Sc in the muddy section of core KSGX 24 may reflect a supplementary oceanic contribution of the sediments provided by marine currents from external sources.

The prevalence of calmer hydrodynamic conditions during longer periods allowed the deposition of the

Table 4. Median and range of element concentrations.

Element	Max.	Min.	Median	Element	Max.	Min.	Median
Al (%)	8.50	5.40	6.10	La (mg kg^{-1})	46	28	37
As (mg kg^{-1})	44	12	18	Li (mg kg^{-1})	101	63	88
Ca (%)	6.00	2.60	4.80	Ni (mg kg^{-1})	62	23	32
Co (mg kg^{-1})	10	6	7	S (%)	1.95	0.44	0.90
Cr (mg kg^{-1})	69	38	53	Sc (mg kg^{-1})	11.5	6.2	7.9
Fe (%)	4.00	2.40	2.90	Sr (mg kg^{-1})	382	198	300
Ga (mg kg^{-1})	21.3	12.8	16.4	V (mg kg^{-1})	98	49	63
K (%)	2.60	1.80	2.10	Zn (mg kg^{-1})	188	64	79

Table 5. Values of the main variables analysed in this study taken in each 2 cm along the core. Dpth – depth (cm), SF – sand fraction (%), FF – fine fraction (%), DM – detrital minerals (%), F/C – "fine detrital minerals versus coarse detrital minerals" ratio, Carb – carbonates (%), Pyr – pyrite (%), I + C – illite + chlorite (%), BFHP (%) and concentrations of Al (%), As (mg kg^{-1}), Ca (%), Co (mg kg^{-1}), Cr (mg kg^{-1}), Fe (%), Ga (mg kg^{-1}), K (%), La (mg kg^{-1}), Li (mg kg^{-1}), Ni (mg kg^{-1}), S (%), Sc (mg kg^{-1}), Sr (mg kg^{-1}), V (mg kg^{-1}) and Zn (mg kg^{-1}).

Dpth	SF	FF	DM	F/C	Carb	Pyr	I+C	BFHP	Al	As	Ca	Co	Cr	Fe	Ga	K	La	Li	Ni	S	Sc	Sr	V	Zn
0	15	85	75	0.4	10	3	12	60	6.9	22	4	10	56	3.5	18	2.3	38	94	35	0.4	9.7	268	76	118
2	15	85	77	0.6	8	3	13	51	6.6	21	4	9	54	3.4	18	2.0	36	93	32	0.6	8.9	267	76	83
4	14	86	81	0.7	9	3	13	59	6.5	23	5	10	59	3.5	19	2.3	40	96	35	0.5	9.5	277	80	94
6	14	86	72	0.6	13	3	15	51	6.7	22	4	9	52	3.4	18	2.2	36	95	32	0.5	8.7	243	77	94
8	14	86	72	0.5	14	3	13	52	6.8	20	4	10	54	3.6	20	2.2	28	96	36	0.7	8.8	241	84	89
10	13	87	78	0.5	12	3	15	51	7.1	22	4	10	56	3.7	20	2.2	30	101	34	0.8	9.4	245	84	86
11	13	87	73	0.6	15	3	16	51	6.8	21	5	10	60	3.5	18	2.2	37	94	35	0.9	8.7	264	73	87
14	16	84	70	0.5	13	5	13	44	6.5	19	4	9	53	3.3	18	2.1	34	91	32	0.9	8.4	255	76	78
16	15	85	76	0.6	13	3	12	52	6.8	22	4	10	53	3.6	18	2.2	30	98	34	1.1	9.3	252	79	83
18	17	83	76	0.5	14	2	10	52	6.9	28	4	10	54	3.5	18	2.3	41	92	35	1.0	9.8	274	72	88
20	18	82	70	0.4	14	4	9	44	6.7	18	5	9	60	3.2	18	2.1	34	88	38	0.9	8.1	284	67	89
22	17	83	72	0.5	16	3	11	43	6.0	16	5	9	46	3.0	17	2.3	35	87	27	0.8	7.9	261	63	86
24	16	84	68	0.2	13	3	12	51	6.3	20	5	9	54	3.2	19	2.1	34	97	34	0.9	8.6	284	66	85
26	17	83	66	0.4	15	3	10	49	6.1	20	5	8	50	3.0	17	2.3	36	89	31	0.9	8.2	283	66	79
28	17	83	72	0.4	16	3	10	48	6.5	18	5	8	50	3.0	17	2.1	38	87	30	0.9	7.9	281	65	81
30	15	85	73	0.5	14	3	12	52	6.4	22	5	9	54	3.1	18	2.2	36	89	34	1.0	8.4	298	67	86
32	19	81	72	0.5	18	3	8	50	5.9	15	5	7	52	2.8	16	2.1	42	77	34	0.8	7.7	301	61	83
34	16	84	71	0.5	17	2	13	54	5.8	18	5	7	65	2.7	17	2.1	40	80	36	0.8	7.8	325	59	76
36	18	82	72	0.5	14	3	9	42	5.7	17	5	10	65	2.6	15	2.0	39	80	34	0.8	7.4	301	58	83
38	18	82	68	0.5	16	3	15	44	5.7	18	5	9	68	2.5	15	2.0	41	76	38	0.8	7.5	329	57	84
40	21	79	63	0.5	23	3	6	48	5.4	14	5	8	56	2.4	15	1.8	41	69	29	0.7	7.0	338	53	72
42	19	81	65	0.4	20	4	8	41	5.5	14	5	8	54	2.4	15	2.0	43	69	27	0.7	6.8	322	54	78
44	20	80	62	0.7	20	4	7	51	5.9	14	6	7	43	2.7	14	2.1	39	69	28	0.8	7.2	319	57	76
46	19	81	71	0.4	16	4	8	44	6.0	14	6	7	49	2.7	15	2.1	45	72	30	0.7	7.3	345	57	80
48	20	80	77	0.5	10	2	7	48	6.1	17	6	7	43	2.7	14	2.1	39	67	25	1.0	7.1	336	57	71
50	21	79	67	0.3	19	3	6	44	6.0	14	6	7	48	2.7	14	2.1	40	68	28	0.8	7.2	330	58	70
52	17	83	68	0.4	16	3	9	53	5.6	14	5	7	44	2.4	14	2.0	41	66	29	0.8	6.6	306	54	67
54	21	79	69	0.5	16	3	6	45	5.8	13	5	6	44	2.4	13	2.0	41	64	28	0.7	6.5	312	51	64
56	18	82	69	0.3	13	3	7	46	6.1	14	6	7	49	2.7	14	2.1	37	70	30	0.7	7.2	328	58	70
58	20	80	73	0.4	10	3	6	50	5.7	13	6	7	47	2.5	14	2.1	44	67	29	0.8	6.9	322	53	68
60	19	81	72	0.5	16	3	5	49	5.9	13	6	7	47	2.6	14	2.0	40	69	29	0.8	7.2	356	54	73
62	24	76	72	0.4	14	3	5	39	5.5	12	6	6	41	2.5	13	1.9	40	63	23	0.8	6.2	339	49	67
64	20	80	71	0.3	13	3	6	50	6.0	13	6	7	45	2.6	15	2.1	43	70	28	0.8	7.4	351	53	78
66	20	80	67	0.5	21	3	6	51	5.5	12	6	7	45	2.6	14	1.9	42	71	24	0.8	6.4	318	52	66
68	20	80	67	0.5	17	4	6	56	6.1	15	5	7	42	2.8	15	2.1	42	74	25	0.9	7.5	317	59	79
70	21	79	55	0.5	9	2	4	46	5.9	15	5	7	44	2.7	16	2.1	38	69	28	0.8	7.1	306	56	72
72	17	83	70	0.4	15	4	8	49	5.9	13	5	7	55	2.6	15	2.0	41	81	35	0.8	7.2	343	55	71
74	15	85	71	0.5	19	3	9	52	5.8	14	5	7	51	2.7	15	2.0	36	84	31	0.8	7.4	311	57	73

Table 5 (Continued).

76	15	85	77	0.4	9	2	10	53	6.0	18	5	8	53	3.0	17	2.2	32	98	31	0.9	8.3	293	65	79
78	16	84	75	0.5	12	3	9	45	5.9	18	5	8	56	2.9	16	2.1	34	93	34	0.9	7.8	306	62	75
80	15	85	68	0.5	15	5	9	59	5.9	18	5	7	56	2.9	16	2.1	41	95	33	0.8	7.8	308	61	79
82	16	84	74	0.6	12	4	10	52	5.9	17	5	7	50	2.8	15	2.1	37	89	29	0.8	7.9	293	59	73
84	18	82	71	0.4	16	4	9	64	5.8	14	5	6	43	2.8	16	2.0	37	89	24	0.8	7.7	284	59	72
86	17	83	80	0.7	9	3	9	48	6.1	15	5	7	52	2.8	16	2.1	37	93	30	0.8	7.5	291	61	77
88	15	85	71	0.6	14	3	9	61	6.0	16	5	7	55	2.8	15	2.0	38	92	32	0.8	7.9	300	63	76
90	15	85	71	0.5	14	3	8	61	6.3	15	5	8	47	2.9	16	2.1	33	94	26	0.8	7.9	287	64	82
92	19	81	74	0.4	14	4	7	58	6.0	17	5	7	44	2.8	15	2.1	40	89	24	0.9	7.5	324	60	74
94	17	83	73	0.7	14	3	8	54	6.0	17	5	7	50	2.8	15	2.0	37	89	29	1.0	7.7	328	61	77
96	17	83	63	0.3	21	1	8	50	5.8	19	5	7	54	2.9	15	2.1	38	86	31	1.0	7.6	307	62	79
98	14	86	73	0.7	15	3	9	51	6.1	16	5	7	51	2.9	16	2.1	40	90	29	1.0	7.6	339	62	79
100	15	85	74	0.8	11	3	7	61	6.0	14	5	8	51	2.9	15	2.0	35	90	27	0.8	7.8	305	62	74
102	15	85	72	0.9	8	4	6	53	6.0	18	5	7	50	3.0	15	2.0	39	87	26	0.9	7.8	299	63	77
104	16	84	72	1.4	12	3	8	60	6.1	16	5	7	55	3.0	16	2.1	37	91	30	0.8	7.9	312	64	73
106	13	87	75	1.2	10	4	8	56	6.3	20	5	7	53	3.2	16	2.1	39	93	29	1.0	8.4	297	69	80
108	14	86	73	0.9	11	3	9	57	6.0	17	5	8	51	3.1	16	2.1	38	89	28	1.0	8.4	295	68	75
110	15	85	81	0.6	9	3	10	55	6.1	15	4	7	49	2.9	15	2.0	39	88	28	0.9	7.9	289	63	74
112	12	88	72	0.7	12	4	12	54	6.4	17	5	7	59	3.1	17	2.1	35	93	36	1.0	8.3	303	68	80
114	16	84	74	0.7	13	4	8	61	6.1	14	5	8	59	3.0	16	2.0	38	88	34	0.9	8.0	303	65	85
116	16	84	68	0.3	15	6	9	55	6.3	18	5	7	57	3.0	15	2.1	40	90	38	1.0	8.1	304	65	82
118	13	87	67	0.9	11	4	11	52	6.3	18	5	9	58	3.2	17	2.1	33	93	35	1.0	8.4	302	72	82
120	13	87	71	0.8	11	5	11	55	6.2	15	5	8	52	3.0	16	2.1	38	91	28	0.9	8.1	319	66	78
122	14	86	70	0.8	11	5	11	51	5.9	18	5	8	53	3.0	16	2.1	37	83	31	1.2	7.5	279	66	79
124	13	87	69	0.9	13	4	11	53	6.0	20	4	8	55	3.0	16	2.1	37	85	30	1.1	7.7	293	67	81
126	15	85	71	1.0	11	4	10	53	6.2	18	5	9	55	2.9	17	2.2	37	90	32	1.1	7.7	315	66	85
128	14	86	73	1.0	11	4	11	63	5.8	17	4	8	49	2.8	17	2.1	39	83	28	0.9	7.3	293	61	77
130	12	88	69	0.9	13	4	12	76	5.9	21	4	8	57	3.0	17	2.1	37	85	37	1.2	7.4	280	67	79
132	12	88	77	0.9	10	4	14	60	6.5	24	4	9	56	3.4	17	2.1	35	91	31	1.2	8.5	257	74	87
134	13	87	68	1.0	13	5	13	70	6.0	23	4	9	53	3.2	16	2.0	32	88	32	1.2	8.2	280	72	188
136	10	90	69	0.8	13	5	16	65	6.1	22	4	8	52	3.2	16	2.0	35	88	31	1.1	8.2	278	71	111
138	11	89	69	1.2	10	4	14	69	6.4	30	4	8	53	3.3	17	2.1	34	92	32	1.4	8.7	269	77	86
140	11	89	76	0.6	12	3	14	56	7.1	27	4	10	60	3.7	18	2.2	35	97	34	1.3	9.9	276	85	95
142	10	90	80	0.9	11	3	15	59	6.9	29	4	9	59	3.6	18	2.2	33	94	33	1.5	9.8	241	84	86
144	9	91	70	0.9	15	4	16	66	7.9	34	4	10	54	3.8	20	2.4	38	92	37	1.6	11.0	248	86	93
146	11	89	78	0.9	8	2	13	62	7.9	31	4	9	50	3.7	19	2.4	37	93	33	1.5	10.8	251	84	96
148	10	90	75	0.9	12	3	15	63	7.5	33	3	9	51	3.4	19	2.3	34	86	35	1.5	10.3	229	84	90
150	11	89	74	0.8	10	3	15	54	8.5	34	3	10	64	3.8	21	2.5	36	97	40	1.6	11.4	234	91	100
152	10	90	75	1.0	10	4	16	61	8.3	37	3	10	57	3.8	20	2.5	38	90	36	1.6	11.0	222	89	93
154	9	91	70	0.9	10	5	18	63	7.4	37	3	9	57	3.8	20	2.4	37	89	37	1.6	10.8	237	89	98
156	11	89	75	1.4	9	4	14	64	7.2	34	4	9	57	3.6	20	2.4	34	90	36	1.5	10.4	245	89	89

Table 5 (Continued).

158	11	89	78	1.0	7	4	17	58	7.7	43	3	9	58	3.8	20	2.4	32	91	36	1.8	10.5	210	93	95
160	9	91	76	0.9	11	3	18	61	8.0	42	3	10	63	3.8	20	2.6	33	96	43	1.9	11.4	213	95	93
162	10	90	80	0.9	7	3	16	53	8.0	42	3	10	62	3.9	21	2.6	33	97	43	1.8	11.5	198	97	101
164	11	89	82	0.8	8	4	15	59	8.0	44	3	10	69	4.0	21	2.6	31	97	47	2.0	11.5	214	98	%
166	9	91	77	0.6	11	3	15	55	6.7	30	3	9	56	3.6	19	2.4	29	87	37	1.6	10.0	226	87	89
168	11	89	78	1.7	7	4	16	57	7.2	33	3	9	59	3.6	19	2.3	31	84	40	1.6	10.1	207	85	94
170	10	90	81	0.7	8	3	15	60	7.3	33	3	10	61	3.8	19	2.4	32	89	41	1.5	10.3	214	88	107
172	11	89	76	0.6	12	3	13	68	6.9	30	4	9	60	3.5	19	2.3	30	87	38	1.2	9.6	256	81	95
174	16	84	73	0.7	12	3	10	44	6.2	19	5	7	56	2.9	17	2.3	36	86	35	0.9	8.3	281	65	80
176	14	86	70	0.7	13	3	12	52	6.9	19	4	8	62	3.1	18	2.3	34	87	41	0.9	9.2	268	69	100
178	14	86	76	0.5	10	3	11	48	6.1	16	5	7	51	2.9	17	2.3	34	88	35	1.0	8.5	292	66	84
180	15	85	73	0.4	14	3	10	54	6.5	16	4	8	47	2.8	17	2.3	37	85	32	0.9	8.8	281	66	129
182	14	86	76	0.5	10	3	11	46	6.3	18	5	8	50	2.9	18	2.3	36	89	34	0.9	8.5	287	69	83
184	13	87	74	0.6	11	2	11	46	6.5	19	4	8	52	2.9	17	2.3	37	85	33	0.9	8.2	280	69	80
186	16	84	75	0.5	14	3	11	50	6.5	28	4	9	55	3.2	18	2.3	36	86	36	1.2	8.9	284	72	85
188	16	84	73	0.6	14	4	11	54	5.9	28	5	7	46	2.7	16	2.2	43	75	30	1.0	7.6	349	62	75
190	17	83	67	0.6	16	4	9	42	5.8	18	5	6	43	2.6	15	2.1	42	74	26	0.8	7.5	367	57	70
192	21	79	69	0.6	18	2	7	50	6.0	18	5	6	46	2.7	17	2.2	44	77	27	0.7	7.8	348	60	72
194	17	83	71	0.6	15	4	10	44	6.0	17	6	7	49	2.6	15	2.2	42	76	32	0.8	7.8	382	59	75
196	21	79	71	0.7	14	4	8	60	5.9	16	6	6	47	2.5	16	2.2	42	72	31	0.8	7.5	368	59	75
198	20	80	73	0.2	6	4	7	48	6.0	14	6	6	43	2.5	15	2.2	46	73	26	0.7	7.6	361	56	70
200	18	82	70	0.6	15	2	7	51	6.1	17	6	6	43	2.6	16	2.2	44	78	28	0.9	7.9	381	58	73
202	19	81	74	0.5	15	2	7	48	5.6	14	5	6	38	2.4	15	2.1	44	72	25	0.7	7.3	357	55	71
204	18	82	68	0.5	17	3	6	53	6.1	15	5	7	47	2.5	16	2.2	43	79	32	0.9	7.2	361	54	71
206	17	83	68	0.6	21	3	7	47	6.1	16	5	7	49	2.6	16	2.3	42	82	32	0.8	7.6	351	56	71
208	18	82	65	0.4	20	5	6	49	5.9	14	5	6	49	2.5	16	2.2	41	77	32	0.7	7.3	337	53	70
210	17	83	71	0.6	16	4	7	52	6.0	17	5	7	42	2.5	16	2.2	43	79	28	0.9	7.5	352	56	73
212	18	82	72	0.5	15	3	7	49	6.4	15	5	6	50	2.6	17	2.3	42	84	31	0.8	7.4	342	55	74
214	17	83	74	0.6	13	3	7	57	6.1	17	5	7	49	2.6	17	2.3	39	85	28	0.9	8.0	343	56	77
216	15	85	78	0.5	12	3	8	62	6.0	16	5	8	60	2.5	16	2.0	32	93	31	0.9	7.1	265	60	76
218	15	85	74	0.5	18	3	9	53	6.2	17	5	6	54	2.5	16	2.2	36	95	30	0.9	7.6	281	60	69
220	15	85	72	0.9	13	3	7	64	6.7	18	5	8	56	2.6	16	2.3	38	99	29	1.0	7.0	300	64	77
222	13	87	67	0.8	14	3	10	58	6.7	19	5	8	60	2.6	16	2.2	37	95	35	1.0	7.5	326	61	77
224	14	86	69	1.0	12	4	10	54	6.8	19	5	7	66	2.7	17	2.3	39	100	37	1.0	7.9	310	62	84
226	16	84	76	0.9	3	5	9	57	6.7	18	5	8	61	2.6	17	2.2	36	96	35	0.9	7.5	317	60	76
228	15	85	72	1.0	11	4	9	47	6.2	16	5	7	56	2.4	15	2.1	40	87	34	0.8	6.7	320	54	70
230	15	85	70	1.1	14	3	8	56	6.6	17	5	6	54	2.6	17	2.1	41	96	62	0.8	7.6	352	57	79
232	18	82	65	0.6	16	5	6	55	6.3	16	5	7	54	2.5	15	2.1	39	89	28	0.8	7.2	309	54	66
234	17	83	74	1.0	10	3	7	51	6.2	19	5	6	50	2.4	15	2.0	40	90	27	0.8	7.3	348	54	72

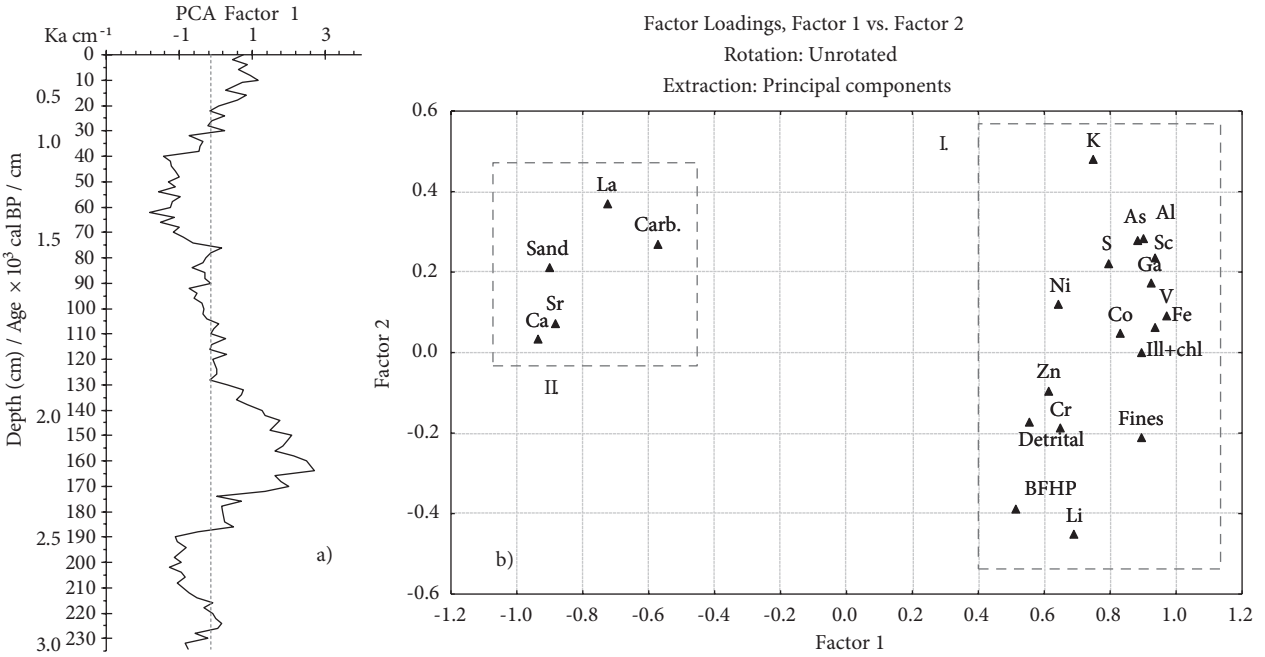

Figure 3. Results of principal components analysis: a) The depth plot of the main factor scores. b) Factor 2 is plotted versus factor 1; variables of group I include percentage of fine fraction (Fines), illite plus chlorite (Ill+chl), detrital minerals (Detrital) and BFHP, and concentrations of Al, As, Co, Cr, Fe, Ga, K, Li, Ni, S, Sc, V and Zn; variables of group II comprise sand fraction (Sand), carbonated minerals (Carb.) and concentrations of Ca, Sr and La.

muddy sections. These conditions may also have been more favourable to the supply of a greater amount of OM, as indicated by the higher values of BFHP. The flux of OM to the bottom is the primary food source for the benthic organisms. OM can be supplied from continental sources or from exported surface water productivity. Benthic foraminifera respond mainly to the high flux of fresh (with high nourishment quality) OM delivered from the biological productivity in the water column (Loubere & Fariduddin 1999; Ernst & van der Zwaan 2004). Biological productivity improves in the Ria de Vigo following the establishment/intensification of the upwelling oceanographic productivity regime (Prego 1993; Tilstone *et al.* 1994, 1999, 2000; Cermeño *et al.* 2006).

Thus, we assume that higher BFHP values may be linked with periods of upwelling established by the prevalence and strengthening of northerly winds and a high flux of OM (Martins *et al.* 2007). The higher concentrations of Fe and S in the muddy sections, where the pyrite amount increases slightly, may also result from processes involved in the formation of pyrite and OM degradation.

The higher deposition of OM during the muddy events also generated lower oxic conditions, which discouraged the development of large populations of exigent benthic organisms (with carbonated shells or tests) due to limited oxygen availability, as suggested by the decrease in carbonate content and Ca and Sr concentrations in these layers.

5.2. Clay mineral assemblages and late Holocene climatic oscillations

Detrital clay mineral composition can reflect both the source area soil and thus the weathering, parent material and climatic factors that produced it, or it can reflect simply a source rock of the same composition (Chamley 1989 and references therein). In the latter case the clay mineralogy will not be a good climatic indicator. However, the source rocks for these sediments consist primarily of granite and schist (Julivert *et al.* 1980). In this case, the clays do, indeed, represent soils developed under the regional climatic regime (as was indicated by for instance by Biscaye 1965; Griffin *et al.* 1968; Millot 1979).

The clay mineral assemblage of the studied site, characterised by the distinct dominance of illite, intermediate concentrations of kaolinite and minor amounts of smectite and chlorite, reflects temperate humid climate conditions prevailing in the source areas where Palaeozoic igneous (granitic rocks) and metamorphic rocks (schists, gneisses, micaschists and greywackes) are abundant (Oliveira *et al.* 2002). High illite and chlorite content may be related to cooler and dryer climates (Griffin *et al.* 1968; Millot 1979).

Illite, a detrital clay mineral that is commonly the product of physical weathering (Chamley 1989), tends to be generally derived from acidic crystalline rocks and is relatively resistant to erosion (Biscaye 1965; Griffin *et*

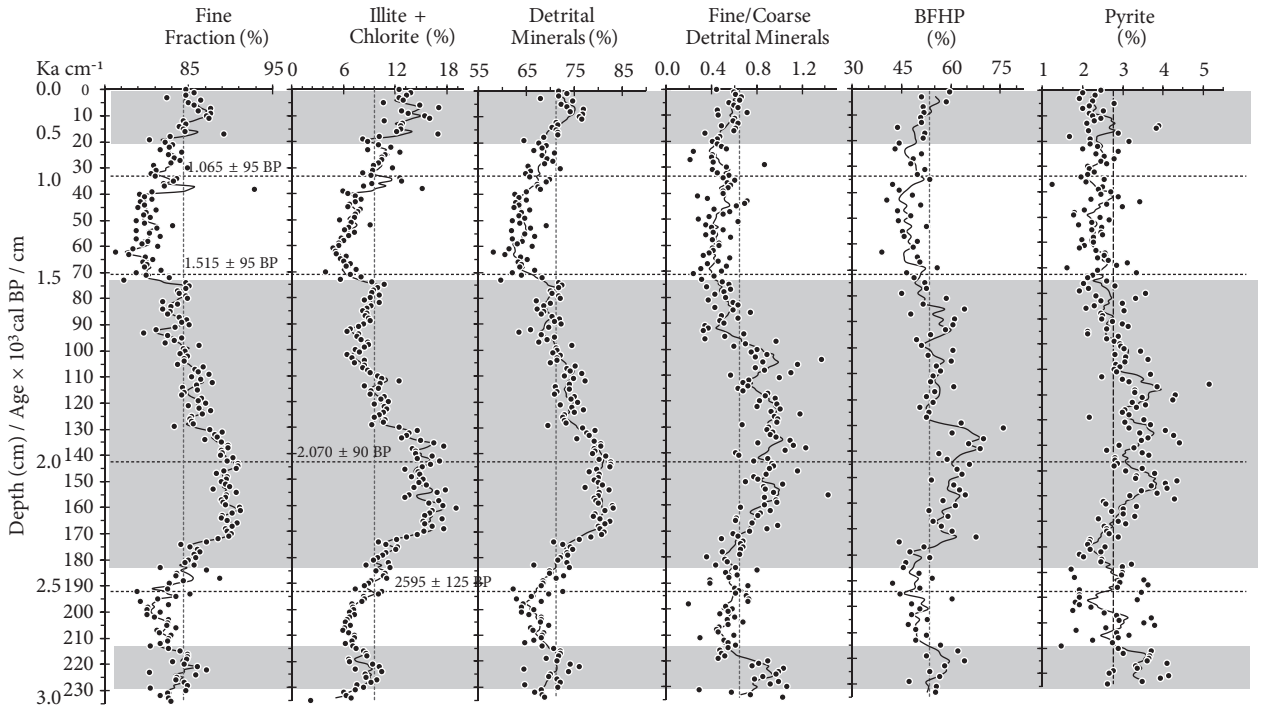

Figure 4. Percentage of fine fraction compared with illite plus chlorite, detrital minerals, BFHP and pyrite in the core. The "fine detrital minerals versus coarse detrital minerals" ratio is also presented. The mean average value (dashed line) and moving averages (solid line between the dots) of each variable are shown, as well as radiocarbon dating (values on the horizontal dashed lines) and a chronological scale (on the left). The muddy sections are shaded in grey.

al. 1968; Windom 1976). There is no evidence that illite can form in situ in the marine environment (Griffin *et al*. 1968; Windom 1976). It is the most abundant clay mineral both on the NW Iberian continental shelf and in fluvial sediments in northern Portugal (Oliveira *et al*. 2002; Drago *et al*. 2006; Abrantes & Rocha 2007).

In the 3 muddy sections (~ 230–214 cm, ~ 185–73 cm and the upper ~ 20 cm; Figure 4), the amount of clay minerals such as illite, kaolinite and chlorite (smectite is rare and without a clear pattern of variation along the core) rises due to the deposition of a high proportion of clay fraction (<2 μm) favoured by weaker bottom currents. However, significant increases in the abundance of illite and chlorite in those layers, which correspond to three very well-known climatic periods, should be caused by a climate effect. The first period may be related to the first cold period of the Upper Holocene, referred to as the northern cold period by Van Geel *et al*. (1996). This climatic oscillation was also identified by the pollen records of the core VIR-18 collected in the central axis of the Ria de Vigo by Desprat *et al*. (2003); the second and third periods may be related to colder phases identified by Álvarez *et al*. (2005) based on coccolith assemblages and biomarkers in that core. These three periods have been also identified by Andrade *et al*. (2011) in the sedimentary record of the outer part of the Ria de Muros (the northernmost of the Rias Baixas).

Bond *et al*. (1992) found a good correlation between colder periods and stronger northerly winds in the Nordic Seas. These core data also suggest that the relatively colder events are associated with the prevalence and strengthening of northerly winds that trigger the upwelling regime as described below.

The upwelling forces a two-layer density-induced positive circulation in the ria, characterised by the inflow of upwelled water through the bottom of the northern mouth and the outflow of surface water through the southern mouth (Crespo *et al*. 2006). Under the upwelling regime the input of the ENACW increases in the ria but in general the introduction of fresh water and the flow of residual current is reduced, particularly during the summer (Prego & Fraga 1992). Upwelled nutrients are efficiently trapped in this system (Álvarez-Salgado *et al*. 1999), favouring biological productivity (Prego 1993; Tilstone *et al*. 1994, 1999, 2000; Cermeño *et al*. 2006). Hence, the ria behaves like an extension of the shelf during the upwelling season and like a partially mixed estuary during the non-upwelling season (Doval *et al*. 1998). A small net exchange from the ria to the shelf occurs under upwelling conditions (Mouriño & Fraga 1985). Oceanic

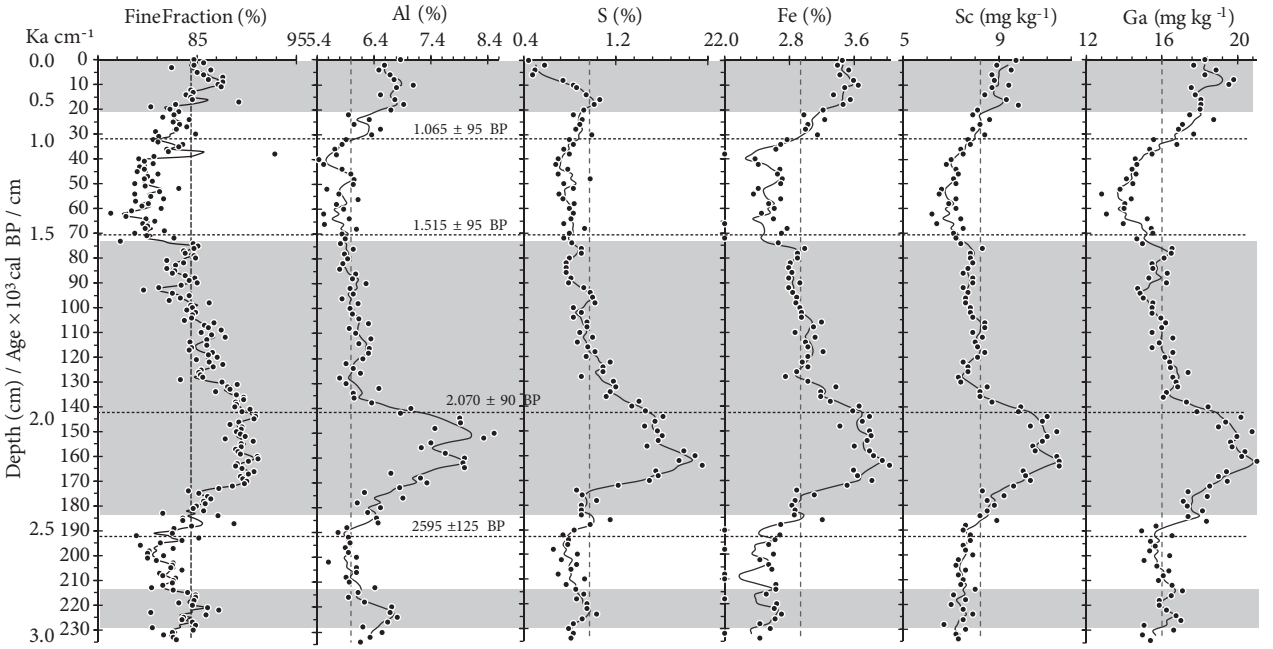

Figure 5. Percentage of fine fraction is compared with Al, S, Fe, Sc and Ga concentrations along the core. The mean average value (dashed line) and moving averages (solid line between the dots) of each variable are shown, as well as radiocarbon dating (values on the horizontal dashed lines) and a chronological scale (on the left). The muddy sections are shaded in grey.

fronts should be formed when deep oceanic water meets waters with greater continental influence in the outer sector of the Ria de Vigo. This interaction generates favourable conditions for the deposition of fine-grained sediments. When strengthened upwelling events occur during the winter, the period with the most rain in this region, and the contribution of sediments from the rivers is higher, the deposition of sediments in the outer sector of the Ria de Vigo may increase.

Thus, periods of higher deposition of finer sediments enriched in detrital minerals and OM contents may be linked to colder climatic oscillations associated with the strengthening of northerly winds and the upwelling regime ~ 2.9 ka cal BP, between ~ 2.2 and 1.2 ka cal BP and from ~ 0.6 ka cal BP. The occurrence of upwelling events, not only during the spring/summer period (the typical situation) but also during the winter, contributed to an increased terrigenous component supplied by the local river system as well as oceanic currents, mostly between ~ 2.2 and 1.2 ka cal BP. Oceanic currents flowing southward can be expected to have transported sediments from northern areas, which is a possible explanation for the higher concentrations of Sc, for example, in the sediments deposited during these periods. This kind of phenomenon is also recorded on the Galician continental shelf (Martins *et al.* 2007).

The intervening periods, between the muddy events, may be related to the prevalence of the winter oceanographic regime. During winter, stronger waves typical occur in the area (PO-WAVES Group, 1994). Southerly and westerly storm winds develop a poleward flow on the shelf and the oceanic jet forces the entry of water, at surface level, into the southern mouth of the Ria de Vigo (Crespo *et al.* 2006). During this season, the ria circulation is characterised by outflow towards the ocean through the bottom of the northern mouth, in an outer circulation cell, while the inner cell maintains a positive circulation forced by river runoff (Crespo *et al.* 2006). Stronger hydrodynamic conditions during winter cause a more vigorous movement and resuspension of bottom sediments. Under these circumstances the finer sediment trap in the outer sector of the Ria de Vigo and the output of fine-grained sediment is greatly reduced.

These results indicate that prevalent periods of continual reinforced upwelling or downwelling may have occurred on a centennial/millennial scale during the late Holocene, as also observed by Diz *et al.* (2002), Álvarez *et al.* (2005), Martins *et al.* (2007) and Andrade *et al.* (2011).

6. Conclusion

Variations in the abundance of illite plus chlorite in the core KSGX 24 suggest the occurrence of relatively cold conditions at ~ 2.9 ka cal BP, between ~ 2.2 and 1.2 ka cal BP and since ~ 0.6 ka cal BP in Galicia. These phases, which are also recorded in other sedimentary records from this region, were probably linked with the reinforced

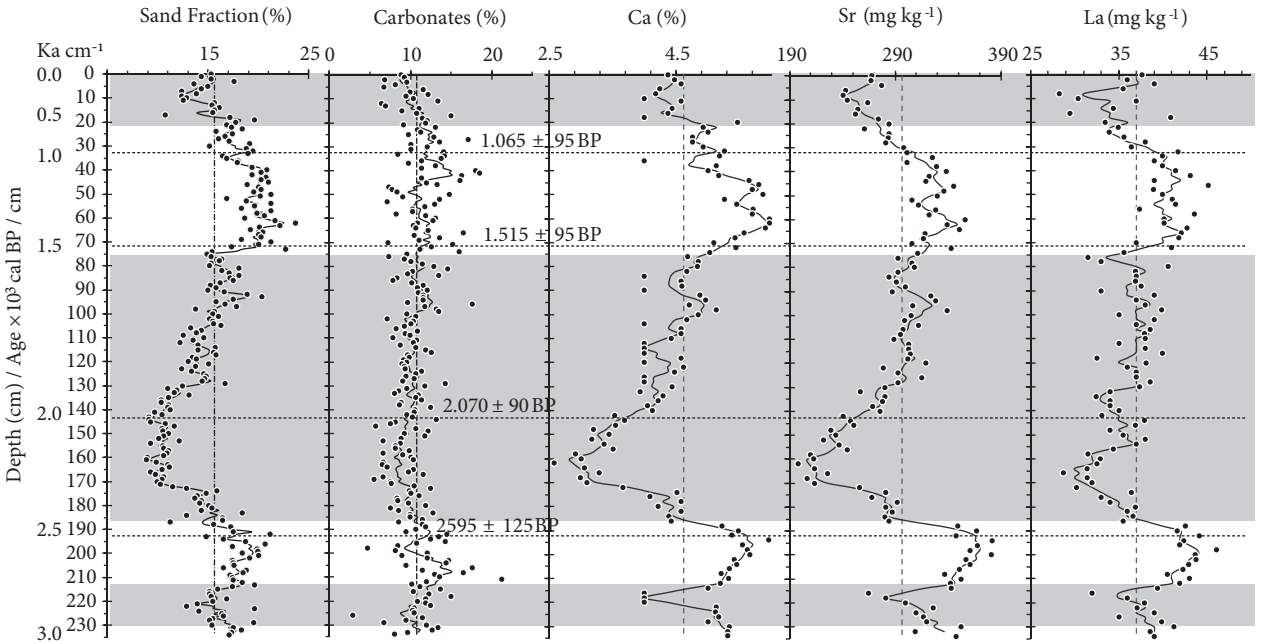

Figure 6. Percentage of sand fraction is compared with the percentage of carbonated minerals and the concentrations of Ca, Sr and La along the core. The mean average value (dashed line) and moving averages (solid line between the dots) of each variable are shown, as well as radiocarbon dating (values on the horizontal dashed lines) and a chronological scale (on the left). The muddy sections are shaded in grey.

northerly winds and the prevalence of the strengthened upwelling regime. These conditions may have promoted a small net exchange between the Ria de Vigo and the shelf and generated an environment suitable for trapping fine-grained sediments in the outer sector of the Ria de Vigo system, which was enriched in OM supplied by biological productivity. During these periods, but mostly between ~ 2.2 and 1.2 ka cal BP, upwelling events probably became more frequent, not only during the spring/summer but also during the winter, when the runoff from the rivers around the ria is higher, producing a larger supply of nearby terrigenous sediments in the study area. The persistent presence of oceanic currents flowing southward on the shelf also brought an increased contribution of terrigenous material from northern continental areas. These climatic oscillations occurred on a centennial/millennial scale and coincide with very well-known climatically cold events (first cold period of the Upper Holocene, Dark Ages and Little Ice Age).

Acknowledgements

The authors would like to thank the 3 anonymous reviewers for collaborating on the improvement of this work. Financial support was granted by the Portuguese Foundation for Science and Technology strategic project PEst-C/CTE/UI4035/2011.

References

Abrantes, I. & Rocha, F. 2007. Sedimentary dynamics of the Aveiro Shelf (Portugal). *Journal of Coastal Research* **SI 50**, 1005–1009.

Álvarez, M.C., Flores, J.A., Sierro, F.J., Diz, P., Francés, G., Pelejero, C. & Grimalt, J. 2005. Millennial surface water dynamics in the Ría de Vigo during the last 3000 years as revealed by coccoliths and molecular biomarkers. *Palaeogeography, Palaeoclimatology, Palaeoecology* **218**, 1–13.

Álvarez-Salgado, X.A., Doval, M.D. & Perez, F.F. 1999. Dissolved organic matter in shelf waters off the Ria de Vigo NW Iberian upwelling system. *Journal of Marine Systems* **18**, 383–394.

Álvarez-Salgado, X.A., Rosón, G., Pérez, F.F., Figueiras, F.G. & Pazos, Y. 1996. Nitrogen cycling in an estuarine upwelling system, the Ría de Arousa NW Spain: I. Short-time-scale patterns of hydrodynamic and biogeochemical circulation. *Marine Ecology Progress Series* **135**, 259–273.

Andrade, A., Rubio, B., Rey, D., Álvarez-Iglesias, P., Bernabeu, A.M. & Vilas, F. 2011. Palaeoclimatic changes during the last 3500 years inferred from diagenetical proxies in the sedimentary record of the Ria de Muros (NW Spain). *Climate Research* **48**, 247–259.

Araújo, M.F., Jouanneau, J.M., Valério, P., Barbosa, T., Gouveia, A., Weber, O., Oliveira, A., Rodrigues, A. & Dias, J.M.A. 2002. Geochemical tracers of northern Portuguese estuarine sediments on the shelf. *Progress in Oceanography* **52**, 277–297.

Belzunce-Segarra, M.J., Wilson, M.J., Fraser, A.R., Lachowski, E. & Duthie, D.M.L. 2002. Clay mineralogy of Galician coastal and oceanic surface sediments: contributions from terrigenous and authigenic sources. *Clay Minerals* **37**, 23–37.

Bender, M.L. & Heggie, D.T. 1984. Fate of organic carbon reaching the deep sea floor: a status report. *Geochimica et Cosmochimica Acta* **48**, 977–986.

Bernárdez, P., González-Álvarez, R., Francés, G., Prego, R., Bárcena, M.A. & Romero, O.E. 2008. Late Holocene history of the rainfall in the NW Iberian peninsula - Evidence from a marine record. *Journal of Marine Systems* **72**, 366–382.

Biscaye, P.E. 1965. Mineralogy and sedimentation of recent deep-sea clay in the Atlantic Ocean and adjacent seas and oceans. *Geological Society American Bulletin* **76**, 803–832.

Biscaye, P.F. 1964. Distinction between kaolinite and chlorite in recent sediments by X-ray diffraction. *American Mineralogist* **49**, 1281–1289.

Bischoff, J.L. & Cummins, K. 2001. Wisconsin glaciation of the Sierra Nevada (79,000–15,000 yr B.P.) as recorded by rock flour in sediments of Owens Lake, California. *Quaternary Research* **55**, 14–24.

Bischoff, J.L., Menking, K.M., Fitts, J.P. & Fitzpatrick, J.A. 1997. Climatic oscillations 10,000–155,000 yr B.P. at Owens Lake, California reflected in glacial rock flour abundance and lake salinity in core OL-92. *Quaternary Research* **48**, 313–325.

Blanton, O., Tenore, K.R., Castillejo, F., Atkinson, L.P., Schwing, F.P. & Lavin, A. 1987. The relationship of upwelling to mussel production in the rias on the Western coast of Spain. *Journal of Marine Research* **45**, 495–511.

Bond, G., Heinrich, H., Broecker, W., Labeyrie, L., McManus, J., Andrews, J., Houn, S., Jantschick, R., Clasen, S., Simet, C., Tedesco, K., Klas, M., Bonani, G. & Ivy, S. 1992. Evidence for massive discharges of icebergs into the North Atlantic ocean during the last glacial period. *Nature* **360**, 245–249.

Castañón, L.G.C., Floor, P., Salinas, F.G., Hurtado, J.A., Navas, J.R. & Palenzuela, J.M.Z. 1981. Mapa Geológico de España (escala 1:50 000). Hoja de Vigo (4-11, 223). Instituto Geológico y Minero de España, Madrid.

Cermeño, P., Maraño, E., Valesca Pérez, V., Serret, P., Fernández, E. & Castro, C.G. 2006. Phytoplankton size structure and primary production in a highly dynamic coastal ecosystem (Ría de Vigo, NW-Spain): Seasonal and short-time scale variability. *Estuarine, Coastal and Shelf Science* **67**, 251–266.

Chamley, H. 1989. Clay sedimentology. Springer-Verlag, New York.

Crespo, B.G., Figueiras, F.G., Porras, P. & Teixeira, I.G. 2006. Downwelling and dominance of autochthonous dinoflagellates in the NW Iberian margin: The example of the Ria de Vigo. *Harmful Algae* **5**, 770–781.

Desprat, S., Sánchez-Goñi, M.F. & Loutre, M.F. 2003. Revealing climatic variability of the last three millennia in northwestern Iberia using pollen influx data. *Earth and Planetary Science Letters* **213**, 63–78.

Diekmann, B., Hofmann, J. Henrich, R., Fütterer, D.K., Röhl, U. & Kuo-Yen, W. 2008. Detrital sediment supply in the southern Okinawa Trough and its relation to sea-level and Kuroshio dynamics during the late Quaternary. *Marine Geology* **255**, 83–95.

Diz, P., Francés, G., Costas, S., Souto, C. & Alejo, I. 2004. Distribution of benthic foraminifera in coarse sediments, Ría de Vigo, NW Iberian Margin. *Journal of Foraminiferal Research* **34**, 258–275.

Diz, P., Francés, G., Pelejero, C., Grimalt, J.O. & Vilas, F. 2002. The last 3000 years in the Ría de Vigo (NW Iberian Margin): climatic and hydrographic signals. *The Holocene* **12**, 459–468.

Diz, P., Francés, G. & Rosón, G. 2006. Effects of contrasting upwelling–downwelling on benthic foraminiferal distribution in the Ría de Vigo (NW Spain). *Journal of Marine Systems* **60**, 1–18.

Doval, M.D., Nogueira, E. & Pérez, F.F. 1998. Spatio-temporal variability of the thermohaline and biogeochemical properties and dissolved organic carbon in a coastal embayment affected by upwelling: the Ria de Vigo (NW Spain). *Journal of Marine Systems* **14**, 135–150.

Drago, T., Freitas, C., Rocha, F., Moreno, J., Cachao, M., Naughton, F., Fradique, C., Araujo, F., Silveira, T., Oliveira, A., Cascalho, J. & Fatela, F. 2006. Paleoenvironmental evolution of estuarine systems during the last 14000 years - the case of Douro estuary (NW Portugal). *Journal of Coastal Research*, **SI 39**, 186–192.

Eby, G.N. 1973. Scandium geochemistry of the Oka Garbonatite Complex, Oka, Quebec. *American Mineralogist* **58**, 819–825.

Ernst, S. & van der Zwaan, B. 2004. Effects of experimentally induced raised levels of organic flux and oxygen depletion on a continental slope benthic foraminiferal community. *Deep Sea Research* Part I, **51**, 1709–1739.

Figueiras, F.G., Labarta, U. & Fernández Reiriz, M.J. 2002. Coastal upwelling, primary production and mussel growth in the Rias Baixas of Galicia. *Hydrobiologia* **484**, 121–131.

Fiúza, A., Macedo, M.E. & Guerreiro, M.R. 1982. Climatological space and time variation of the Portuguese coastal upwelling. *Oceanologica Acta* **5**, 31–40.

Frondel, C. 1970. Scandium. *In*: Wedepohl, K.H. (ed), *Handbook of Geochemistry*. Springer-Verlag, Berlin.

Galhano, C., Rocha, F. & Gomes, C. 1999. Geostatistical analysis of the influence of textural, mineralogical and geochemical parameters on the geotechnical behaviour of the "Argilas de Aveiro" formation (Portugal). *Clay Minerals* **34**, 109–116.

García-García, A., García-Gil, S. & Vilas, F. 2005. Quaternary evolution of the Ria de Vigo, Spain. *Marine Geology* **220**, 153–179.

González-Álvarez, R., Bernárdez, P., Pena, L.D., Francés, G., Prego, R., Diz, P. & Vilas, F. 2005. Paleoclimatic evolution of the Galician continental shelf (NW of Spain) during the last 3000 years: from a storm regime to present conditions. *Journal of Marine Systems* **54**, 245–260.

Griffin, J.J., Windom, H. & Goldberg, E.D. 1968. The distribution of clay minerals in the world oceans. *Deep-Sea Research* **15**, 433–459.

Haynes, R. & Barton, E.D. 1990. A poleward flow along the Atlantic coast of the Iberian Peninsula. *Journal of Geophysical Research* **95**, 11425–11441.

Hurtado, J.A., Salinas, F.G., Dones, V.P., Navas, J.R., Menéndez, J.B.S., Castañón, L.G.C. & Floor, P. 1981. Mapa Geológico de España (escala 1:50 000). Hoja de Tuy (4-12, 261). Instituto Geológico y Minero de España, Madrid.

Jason, R., Price, J.R., Velbel, M.A. & Patino, L.C. 2005. Rates and time scales of clay-mineral formation by weathering in saprolitic regoliths of the southern Appalachians from geochemical mass balance. *Bulletin of the Geological Society of America* **117**, 783–794.

Jouanneau, J.M., Weber, O., Drago, T., Rodrigues, A., Oliveira, A., Dias, J.M.A., Garcia, C., Schmidt, S. & Reyss, J.L. 2002. Recent sedimentation and sedimentary budgets on the western Iberian shelf. *Progress in Oceanography* **52**, 261–275.

Julivert, M., Martinez, F.J. & Ribeiro, A. 1980. The Iberian segment of the European Hercynian Foldbelt, in Geology of Europe from Precambrian to the Post-Hercynian Sedimentary Basins. Bureau de Recherches Géologiques et Minières Société Géologique du Nord, 132–158.

Loring, D.H. 1990. Lithium — a new approach for the granulometric normalization of trace metal data. *Marine Chemistry* **29**, 155–168.

Loring, D.H. 1991. Normalization of heavy-metal data from estuarine and coastal sediments. *ICES Journal of Marine Science* **48**, 101–115.

Loubere, P. & Fariduddin, M. 1999. Benthic Foraminifera and the flux of organic carbon to the seabed. *In*: Sen Gupta, B.K. (ed), *Modern Foraminifera*, Kluwer Academic Publishers, Dordrecht/Boston/London, 181–199.

Martínez-Ansemil, E. & Membiela, P. 1992. The low mineralized and fast turnover watercourses of Galicia. *Limnetica* **8**, 125–130.

Martins, V., Dubert, J., Jouanneau, J.M., Weber, O., Silva, E.F., Patinha, C., Dias, J.M.A. & Rocha, F. 2007. A multiproxy approach of the Holocene evolution of shelf–slope circulation on the NW Iberian Continental Shelf. *Marine Geology* **239**, 1–18.

Martins, V., Jouanneau, J.M., Weber, O. & Rocha, F. 2006a. Tracing the late Holocene evolution of the NW Iberian upwelling system. *Marine Micropaleontology* **59**, 35–55.

Martins, V., Patinha, C., Ferreira da Silva, E., Jouanneau, J.M., Weber, O. & Rocha, F. 2006b. Holocene record of productivity in the NW Iberian continental shelf. *Journal of Geochemical Exploration* **88**, 408–411.

Martins, V., Rocha, F., Jouanneau, J., Weber, O., Gomes, C., Dias, J. & Gomes, V. 2005. Geochemical, textural, mineralogical and micropaleontological data used for climatic reconstruction during the Holocene in the Galicia sector of the Iberian Continental Margin. *Ciências Marinas* **31**, 293–307.

Menking, K.M. 1997. Climatic signals in clay mineralogy and grain-size variations in Owens Lake core OL-92, southeast California. GSA Special Papers **317**, 25–36.

Millot, G. 1979. Geology of Clays. Springer-Verlag, Berlin.

Mohamed, K., Rey, D., Rubio, B., Dekkers, M., Roberts, A.P. & Vilas, F. 2011. Onshore–offshore gradient in reductive early diagenesis in coastal marine sediments of the Ria de Vigo, Northwest Iberian Peninsula. *Continental Shelf Research* **31**, 433–447.

Mouriño, C. & Fraga, F. 1985. Determinación de nitratos en agua de mar. *Investigaciones Pesqueras* **49**, 81–96.

Norman, J.C. & Haskin, L.A. 1968. The geochemistry of Sc: A comparison to the rare earths and Fe. *Geochimica et Cosmochimica Acta* **32**, 93–108.

Oliveira, A., Rocha, F., Rodrigues, A., Jouanneau, J.M., Dias, A., Weber, O. & Gomes, C. 2002. Clay minerals from the sedimentary cover from Northwest Iberian shelf. *Progress in Oceanography* **52**, 233–247.

Peliz, Á., Rosa, T.L., Miguel, A., Santos, P. & Pissarra, J.L. 2002. Fronts, jets, and counter-flows in the Western Iberian upwelling system. *Journal of Marine Systems* **35**, 61–77.

Pérez-Arlucea, M., Mendez, G., Clemente, F., Nombela, M., Rubio, B. & Filgueira, M. 2005. Hydrology, sediment yield, erosion and sedimentation rates in the estuarine environment of the Ria de Vigo, Galicia, Spain. *Journal of Marine Systems* **54**, 209–226.

Pondal, P.I., Vegas, R. & Marcos, A. 1982. Notas explicativas al mapa geológico do Macizo Hespérico, escala 1:500 000. Publicacións da Área de Xeoloxía e Minería do Seminario de Estudos Galegos.

PO-WAVES Group. 1994. Final report of sub-project A, Wind wave climatology of the Portuguese coast. Instituto Hidrográfico, REL. FT.OM 5/94.

Prego, R. 1993. General aspects of carbon biogeochemistry in the Ría de Vigo, northwestern Spain. *Geochimica et Cosmochimica Acta* **57**, 2041–2052.

Prego, R. & Fraga, F., 1992. A simple model to calculate the residual flows in a Spanish ria. Hydrographic consequences in the ria of Vigo. *Estuarine, Coastal and Shelf Science* **34**, 603–615.

Rubio, B., Nombela, M.A. & Vilas, F. 2000. Geochemistry of major and trace elements in sediments of the Ria de Vigo (NW Spain): an assessment of metal pollution. *Marine Pollution Bulletin* **40**, 968–980.

Saleh, G.M. 2007. Geology and rare-earth element geochemistry of highly evolved, molybdenite-bearing granitic plutons, Southeastern Desert, Egypt. *Chinese Journal of Geochemistry* **26**, 333–344.

Soares, A.M.M. & Dias, J.M.A. 2007. Reservoir effect of coastal waters off Western and Northwestern Galicia. *Radiocarbon* **49**, 925–936.

Stuiver, M. & Reimer, P.J. 1993. Extended ^{14}C data base and revised CALIB 3.0 ^{14}C age calibration program. *Radiocarbon* **35**, 215–230.

Tenore, K.R., Alonso-Noval, M., Álvarez-Ossorio, M., Atkinson, L.P., Cabanas, J.M., Cal, R.M., Campos, H.J., Castillejo, F., Chesney, E.J., Gonzalez, N., Hanson, R.B., McClain, C.R., Miranda, A., Roman, M.R., Sánchez, J., Santiago, G., Valdés, L., Varela, M. & Yoder, J. 1995. Fisheries and oceanography off Galicia, NW Spain: mesoscale spatial and temporal changes in physical processes and resultant patterns of biological productivity. *Journal of Geophysical Research* **100** (C6), 10943–10966.

Thamban, M., Purnachandra Rao, V. & Schneider, R.R. 2002. Reconstruction of late Quaternary monsoon oscillations based on clay mineral proxies using sediment cores from the western margin of India. *Marine Geology* **186**, 527–539.

Tilling, R., Greenland, P.L. & Gottfried, D. 1969. Distribution of scandium between coexisting biotite and hornblende in igneous rocks. *Geological Society of America Bulletin* **80**, 661–658.

Tilstone, G.H., Figueiras, F.G., Fermin, E.G. & Arbones, B. 1999. Significance of nanophytoplankton photosynthesis and primary production in a coastal upwelling system (Ría de Vigo, NW Spain). *Marine Ecology Progress Series* **183**, 13–27.

Tilstone, G.H., Figueiras, F.G. & Fraga, F. 1994. Upwelling-downwelling sequences in the generation of red tides in a coastal upwelling system. *Marine Ecology Progress Series* **112**, 241–253.

Tilstone, G.H., Míguez, B.M., Figueiras, F.G. & Fermín, E.G. 2000. Diatom dynamics in a coastal ecosystem affected by upwelling: coupling between species succession, circulation and biogeochemical processes. *Marine Ecology Progress Series* **205**, 23–41.

Torre, E. 1958. Estado actual del conocimiento de las Rías gallegas. *In*: Otero Pedrayo, R. (ed), *Homenaje a Otero Pedrayo*. Galaxia, Vigo, 237–250.

Van Geel, B., Buurman, J. & Waterbolk, H.T. 1996. Archaeological and palaeoecological indications of an abrupt climate change in the Netherlands, and evidence for climatological teleconnections around 2650 BP. *Journal of Quaternary Science* **11**, 451–460.

Vidal Romani, J.R. 1984. A orixe das Rías Galegas. Estado da cuestion (1986-1983). *Cuadernos da Area de Ciencias Marinas de Estudos Galegos* **1**, 13–25.

Vidinha, J., Rocha, F., Andrade, C., Gomes, C., & Freitas, C., 2007. Clay minerals - a mineralogical tool to distinguish beach from dune sediments. *Journal of Coastal Research*, **SI 50**, 216–220.

Vilas, F., Bernabeu, A.M. & Méndez, G., 2005. Sediment distribution pattern in the Rias Baixas (NW Spain): main facies and hydrodynamic dependence. *Journal of Marine Systems* **54**, 261–276.

Vitorino, J., Oliveira, A., Jouanneau, J.M. & Drago, T., 2002. Winter dynamics on the northern Portuguese shelf. Part 1: physical processes. *Progress in Oceanography* **52**, 129–153.

Windom, H.L. 1976. Lithogeneous material in marine sediments. *In:* Riley, J.P. & Chester, R. (eds), *Chemical Oceanography*. Academic Press, London, 103–135.

Wooster, W.S., Bakun, A. & McLain, D.R. 1976. The seasonal upwelling cycle along the eastern boundary of the North Atlantic. *Journal of Marine Research* **34**, 131–141.

Yuretich, R. & Ervin, C. 2002. Clay minerals as paleoenvironmental indicators in two large lakes of the African rift valleys: Lake Malawi and Lake Turkana. *In:* Renaut, R.W. & Ashley, G.M. (eds.), *Sedimentation in Continental Rifts* **73**, 221–232.

Yuretich, R., Melles, M., Sarata, B. & Grobe, H. 1999. Clay minerals in the sediments of Lake Baikal; a useful climate proxy. *Journal of Sedimentary Research* **69**, 588–596.